7-1-2016

Symmetries in the time-averaged dynamics of stochastic models of networks dynamics

Abu Bakar Siddique

Abu Bakar Siddique

Candidate

Mechanical Engineering

Department

This thesis is approved, and it is acceptable in quality and form for publication:

Approved by the Thesis Committee:

Dr. Francesco Sorrentino

, Chairperson

Dr. Yu-Lin Shen

Dr. Asal Naseri Kouzehgarani

Symmetries in the time-averaged dynamics of stochastic models of networks dynamics

by

Abu Bakar Siddique

B.Sc., Bangladesh University of Engineering and Technology, 2006

THESIS

Submitted in Partial Fulfillment of the
Requirements for the Degree of

Master of Science in Mechanical Engineering

The University of New Mexico

Albuquerque, New Mexico

July, 2016

Dedication

To my parents, wife and daughter, for their support, encouragement and happy faces.

Acknowledgments

I would like to thank my advisor, Professor Francesco Sorrentino, for his support and directions throughout my research. I would also like to thank Dr. Louis M. Pecora[1], Professor Jorge Orozco-Mora[2], Professor Elvia Ruiz Beltrán[2] and my colleagues for their inputs to my research.

Symmetries in the time-averaged dynamics of stochastic models of networks dynamics

by

Abu Bakar Siddique

B.Sc., Bangladesh University of Engineering and Technology, 2006

M.S., Mechanical Engineering, University of New Mexico, 2016

Abstract

In recent years a large body of research has investigated the dynamics of complex networks, including percolation [1, 2], epidemics [3, 4], synchronization [5, 6], evolutionary game theory [7, 8], and traffic dynamics [9, 10, 11]. These study apply to technological networks, biological networks, and social networks. In general, it has been shown that the topology of these networks (e.g. the degree distribution [12, 13], degree correlation [14, 15], community structure [16], etc.) plays a significant role in their dynamical time evolution.

Keywords: symmetry; dynamical systems; complex networks

Contents

Contents

Contents

List of Figures

List of Figures

List of Tables

Chapter 1

Introduction

1.1   Outline

The presence of symmetries is a very common feature in nature. Almost everywhere in nature we see the symmetries. Symmetries are present in the real networks[21] as well i.e. technological, social, biological etc. And this feature of network topology plays an important role in the evolution of a dynamical model on the network but this is still remained somewhat unexplored with some exceptions[5, 22, 23, 24]. So we considered it as an important research area where we tried to find the possible effects of symmetries on the network dynamics.

References [5, 22, 23, 24] have focused on the effect of the network symmetries on the emergence of cluster synchronization. In our current research, we studied several types of widely studied dynamical models on networks and try to illustrate the effects of the underlying network symmetries on each one of those models. Our study indicates that these symmetries affect the dynamics in all three of the dynamical models considered and suggest that this may be a general feature of several complex networks, independent of the particular type of dynamics considered, though the particular effect of the symmetries may

vary based on the particular dynamics considered.

References [5, 24] studied the case that the network is formed of coupled nonlinear oscillators and showed that the underlying network symmetries determine the emergence of synchronized clusters. In our current research, we consider models characterized by different types of dynamics, either deterministic or probabilistic, which determine the time evolution of the network nodes. We will retain the assumptions that the systems are equal and the connections are equivalent to each other and will show that the symmetries play an important role on the dynamics in all the models considered, including evolutionary games, propagation of excitation, and epidemics.
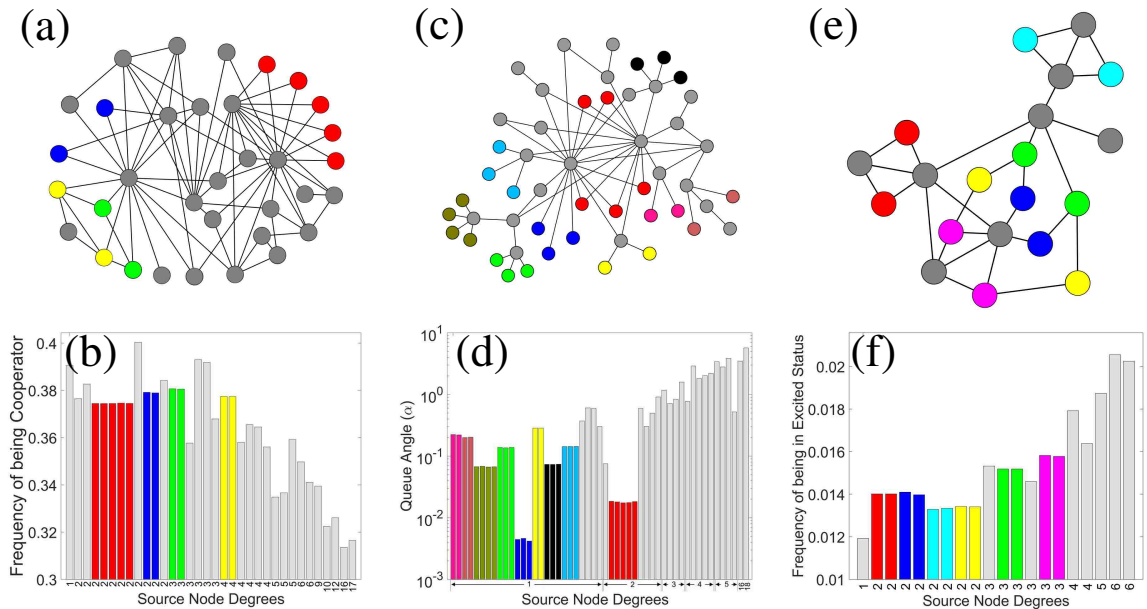
Figure 1.1: Effects of the network symmetries in three different dynamical models/networks: (a-b) Evolutionary game theory played on Zachary's Karate Club Network [17]. (c-d) Network traffic model simulated on Bellsouth network [18]. (e-f) random ER graph and fraction of times each node of this network spends in the excited state according to the Kinouchi Copelli model [19] of excitable systems. In (a), (c), and (e), nodes colored the same are in the same cluster except the gray colored nodes, each of which is in a cluster by itself.

Here, the topology of a network is described by the adjacency matrix $A = \{A_{ij}\}$, where

$A_{ij} = A_{ji}$ is equal to 1 if node j and i affect each other and is equal to 0 otherwise. The symmetries of the network form a (mathematical) group $\mathscr{G}$. Each element of the group can be described by a permutation matrix Π that re-orders the nodes in a way that leaves the network structure unchanged (that is, each Π commutes with A, $\Pi A = A\Pi$). The set of symmetries (or automorphisms) of a network can be quite large, even for small networks, but it can be calculated from knowledge of the matrix A by using widely available discrete algebra routines. In fact, while in certain cases it is possible to identify the symmetries by inspection, in general for an arbitrary network, for which the symmetries may be *hidden*, the use of a software is required. In our current study, we used SageMath [25], an open-source mathematical software. Once the symmetries are identified, the nodes of the network can be partitioned into M clusters by finding the orbits of the symmetry group, i.e., the disjoint sets of nodes that when all of the symmetry operations are applied permute among one another in the same set.

For the current study we have considered three examples of undirected networks, shown in Figs. 1.1(a), (c) and (e): the Zachary's Karate Club network [17] of $N = 34$ nodes, the Bell South network [26] of $N = 51$ nodes and a randomly generated ER graph of $N = 20$ nodes, respectively. Each node of the Karate Club network is a member of a university karate club and a connection represents a friendship relation between them. The nodes of the Bell South network are the IP/MPLSs (Multiprotocol Label Switching: a switching mechanism used in high-performance telecommunications networks). In Fig. 1.1 the colors of the nodes indicate the clusters they belong to, either non trivial (i.e. clusters with more than one node in them) or trivial clusters (clusters with only one node in them). All the nodes in trivial clusters are colored gray while the non-trivial clusters are colored differently. The Karate club network in Fig. 1.1(a) has $C = 4$ nontrivial clusters, and 23 trivial clusters. The Bell South network in Fig. 1.1(c) displays $C = 9$ nontrivial clusters, and 24 trivial clusters. The random network in Fig. 1.1(e) has $C = 6$ non-trivial clusters and 8 trivial clusters. As we will see, each dynamical system will be applied to each network yielding 9 scenarios.

Chapter 2

Symmetries in the Networks

2.1 Basic Terminologies

Network: Network is, in simplest form, a collection of points (vertices or nodes) joined together in pairs by lines (links, edges or bonds). i.e. lattices, random graphs, small world networks, scale-free networks.

A complex network is a graph (network) with non-trivial topological features and network topology is the arrangement of the various elements (links, nodes, etc.) of a network.
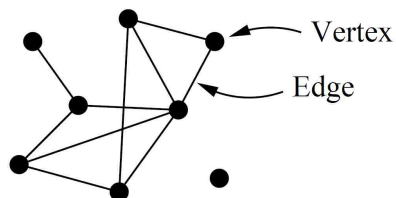
Figure 2.1: A small network composed of eight vertices and ten edges.

Adjacency Matrix: An adjacency matrix is a square matrix used to represent a Network topology. The elements of the adjacency matrix indicate whether pairs of vertices are adjacent or not in the graph. It also shows the weight of each links between two vertices. Example of an undirected and unweighted graph:

$$A_{ij} = \begin{cases} 1 & \text{if there is an edge between vertices } i \text{ and } j \\ 0 & \text{otherwise.} \end{cases}$$
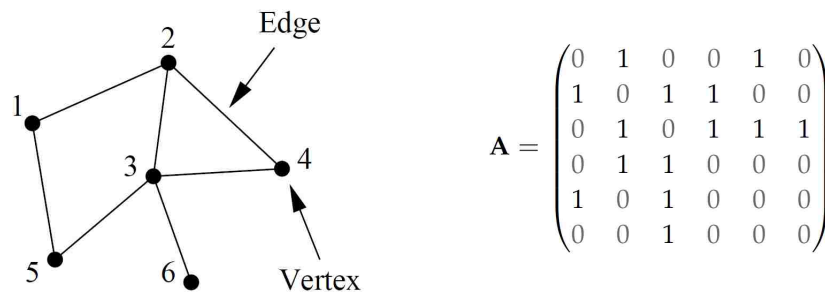
Figure 2.2: A simple network and its adjacency matrix

2.2 Symmetry

Group theory is the study of symmetry. A *Group* is an algebraic structure $(G, \star)$ that has four basic properties:

- Closure: $a, b \in G \rightarrow a \star b \in G$

- Associativity: $(a \star b) \star c = a \star (b \star c)$

- Identity: $\exists e \, (a \star e \equiv e \star a = a)$

- Inverse: $\forall a \exists \left(a \star a^{-1} = a^{-1} \star a = e \right)$

Suppose we have a group $(G, \star)$, and let H be a non-empty subset of G. If $(H, \star)$ is also a group then $(H, \star)$ is a sub-group of $(G, \star)$.

Isomorphism: Two graph G and H are *isomorphic* if there is a bijection $\theta : V(G) \rightarrow V(H)$ which preserve adjacency and non-adjacency.

Figure 2.3: Isomorphism

Homomorphism: A *Homomorphism* from a graph G to a graph H is a mapping (not necessarily bijective) $\alpha : V(G) \rightarrow V(H)$ such that $xy \in E(G) \rightarrow \alpha(x)\alpha(y) \in E(H)$.
 That means,

Figure 2.4: Homomorphism

- α maps edges to edges.

- α may map a non-edge to

    - a single vertex

- an edge

- a non-edge

In Fig. 2.4 all the edges of *G* is mapped into *H* but non-edge *eb* of *G* is mapped into edge 32 of *H* and non-edge *bd* of *G* was mapped into a single vertex 2 of *H*.

Automorphism   An *automorphism* of graph *G* is

- an *isomorphism* between *G* and itself.

- a permutation $\alpha : V(G) \to V(G)$ such that it preserves adjacency and non-adjacency.

- describes the symmetries of the graph.

The set of all automorphisms of a graph *G*, under the operation of composition of functions, forms a subgroup of the symmetric group on $V(G)$ called the automorphism group of *G*, and it is denoted $Aut(G)$.

K_3:
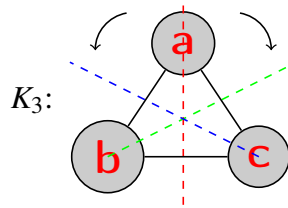
Figure 2.5: Automorphisms

The automorphisms of the graph K_3 are:

- identity, $\varepsilon = (a)(b)(c)$

- reflection, $\alpha_1 = (a)(bc)$

- reflection, $\alpha_2 = (b)(ac)$

- reflection, $\alpha_3 = (c)(ab)$

- rotation, $r_1 = (abc)$

- rotation, $r_2 = (acb)$

Then, $Aut(K_3) = \{\varepsilon, \alpha_1, \alpha_2, \alpha_3, r_1, r_2\}$.

Orbit of an Automorphism Group A relation $\sim$ on a set $(a, b, c) \in V$ is called an equivalence relation if it is reflexive, symmetric and transitive.

- Reflexive: $\forall a$ in s it holds that $a \sim a$

- Symmetric: $\forall (a, b)$ in s it holds that if $a \sim b$ then $b \sim a$

- Transitive: $\forall (a, b, c)$ in s it holds that if $a \sim b$ and $b \sim c$ then $a \sim c$
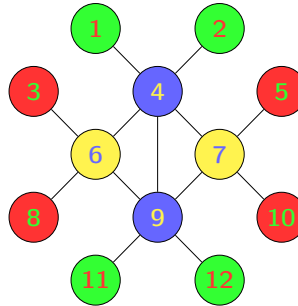
Figure 2.6: Colors showing the Orbits of Automorphism Group

If $\sim$ is an equivalence relation on V, then [u], the equivalence class of u is defined by $[u] = \{v \in V | u \sim v\}$. The orbit of an element is an equivalent class. Let $\mathscr{G}$ be a group permutation of a set V, For each $v \in V$ the orbit of v, denoted by $\mathscr{O}_{\mathscr{G}}(v)$, is the subset of V such that $\mathscr{O}_{\mathscr{G}}(v) = \{u \in V | \exists g \in \mathscr{G}\}$ such that $gv = u$. In Fig. 2.6 different colors show the different orbits of automorphism group.

Chapter 3

Dynamical Experiments

We are interested in observing and characterizing the overall effect of the network symmetries in different scenarios, each of which corresponds to a particular *dynamics* taking place on a network.

3.1 Evolutionary Game Theory

In this dynamical scenario each one of the network nodes (agents) iteratively plays a version of the Prisoner's Dilemma game [7]. Each node i can either be a cooperator ($S_i = 1$) or a defector ($S_i = 0$). The network connectivity is described by the matrix A, where $A_{ij} = 1$ when agent j is connected to agent i, otherwise $A_{ij} = 0$. We define a payoff between two players based on the "Prisoner's Dilemma" game. There are two types of strategy adopted by the players: *cooperation* and *defection*. A cooperator pays a cost c for each one of the agents it is connected to and a defector pays nothing [7]. Each node receives a benefit equal to b for each cooperator it is connected to. When playing the game, node i receives a payoff equal to $\xi_i = \sum_j (A_{ij} b S_j - A_{ji} c S_i)$. We define the fitness [7] of each node to be $f_i = 1 - \omega + \omega \xi_i$, where $0 \leq \omega \leq 1$ measures the intensity of selection. $\omega \simeq 1$ means

strong selection, that is the fitness is almost equal to the payoff and $\omega \simeq 0$ means weak selection, that is the fitness is almost independent of the payoff and close to 1. The literature [7, 27, 28, 29] focuses on the case of weak selection, which is also what we consider here (in all our simultions we set $\omega = 0.1$). Following [7] we choose a death-birth updating rule for the game evolution. Namely, in each time step a random node i is selected to be replaced by a new offspring (node). The new offspring evolves into either a cooperator or a defector depending on the fitness of the surrounding agents. We set the probability of that new node to be a cooperator to be $\sigma(F_{Ci} - F_{Di})$, where F_{Ci} and F_{Di} are the fitnesses of cooperators and defectors in the neighboring nodes and σ is a monotonically increasing function such that $0 \leq \sigma \leq 1$. This reflects a higher propensity of turning into a cooperator based on how *well* the neighbors of a given node that are cooperators are doing with respect to the other neighbors of that node that are defectors. The total fitness of the neighbors of player i is equal to

$$F_i = \sum_{j=1}^{N} A_{ij} f_j \tag{3.1}$$

The fitness of the cooperators and defectors in the neighboring nodes of i is defined as,

$$F_{Ci} = \sum_{j=1}^{N} A_{ij} S_j f_j = \sum_j A_{ij} S_j (1 - \omega) + \omega \sum_j A_{ij} S_j \xi_j$$

$$F_{Di} = F_i - F_{Ci} = \sum_{j=1}^{N} A_{ij}(1 - S_j)(1 - \omega) + \omega \sum_j A_{ij}(1 - S_j)\xi_j \tag{3.2}$$

Letting, $x_i = (F_{Ci} - F_{Di})$, we write the probability that the new offspring will be a cooperator $\sigma(x_i)$. Here we set $\sigma(x_i) = \gamma x_i + \varepsilon$, where $\gamma > 0$ and ε are two arbitrary constants. In all our numerical simulations we have chosen the values of γ and ε so as to ensure $0 \leq \sigma \leq 1$ for all i's. Since in each time step a randomly chosen node out of the N players is selected to update its strategy, we can write,

$$S_i^{t+1} = \begin{cases} S_i^t & \text{with probability } \frac{N-1}{N} \\ 1 & \text{with probability } \frac{1}{N}\sigma(x_i) \\ 0 & \text{with probability } \frac{1}{N}(1 - \sigma(x_i)) \end{cases}$$

From this equation, we can compute the expected value of S_i at time $t+1$,

$$\langle S \rangle_i^{t+1} = \frac{N-1}{N} \langle S \rangle_i^t + \frac{1}{N} \langle \sigma(x_i) \rangle, \tag{3.3}$$

where the symbol $\langle \cdots \rangle$ indicates an average over several realizations. By using $\langle \sigma(x_i) \rangle = \sigma(\langle x_i \rangle)$, Eq. (3.3) becomes,

$$\langle S \rangle_i^{t+1} - \langle S \rangle_i^t = -\frac{1}{N} \left(\langle S \rangle_i^t - \sigma(\langle x_i \rangle) \right) \tag{3.4}$$

The quantity $\langle x_i \rangle = (2\langle F_{Ci} \rangle - \langle F_i \rangle)$ and from Eqs. (3.2) and (3.1) we see that

$$\langle F_i \rangle = \sum_{j=1}^{N} A_{ij} \langle f_j \rangle = \sum_{j=1}^{N} A_{ij} \left[1 - \omega + \omega \langle \xi_j \rangle \right] \tag{3.5}$$

and

$$\langle F_{ci} \rangle = \sum_{j=1}^{N} A_{ij} \langle S_j f_j \rangle = \sum_{j=1}^{N} A_{ij} \langle S_j \rangle \langle f_j \rangle = \sum_{j=1}^{N} A_{ij} \langle S_j \rangle \left[1 - \omega + \omega \langle \xi_j \rangle \right] \tag{3.6}$$

where in order to obtain (3.6) we have made use of the assumption that S_j and f_j are statistically independent. The assumption of statistical independence is reasonable if the network has few short loops and low average degree, see e.g. [2], [30]. For the Bellsouth network the value of average node degree is 2.59 and our numerical results also showed the consistency of this assumption.

In vector form, Eq. (3.4) becomes

$$\langle \mathbf{S} \rangle^{t+1} - \langle \mathbf{S} \rangle^t = -\frac{1}{N} \left(\langle \mathbf{S} \rangle^t - \sigma(\langle \mathbf{x} \rangle) \right) \tag{3.7}$$

where the vectors $\langle \mathbf{x} \rangle = \langle \mathbf{F_C} \rangle - \langle \mathbf{F_D} \rangle = 2\langle \mathbf{F_C} \rangle - \langle \mathbf{F} \rangle$, $\mathbf{S} = [S_1, S_2, \ldots, S_N]$, $\mathbf{F} = [F_1, F_2, \ldots, F_N]$ and $\mathbf{F_C} = [F_{C1}, F_{C2}, \ldots, F_{CN}]$. We see that at steady state, $\langle \mathbf{S} \rangle = \sigma(\langle \mathbf{x} \rangle)$.

We see that Eq. (3.7) can be solved iteratively at steady state in the unknown quantities $\langle S \rangle_i$, $i = 1, 2, \ldots, N$. This is shown in Fig. 4.4(a) where $\langle S \rangle_i$ obtained by the iterative solution of Eq. (3.7) at steady state is plotted versus the value of $\langle S \rangle_i$ obtained from the numerical simulation of the game averaged over a number of realizations colors are consistent with Fig. 1.1(a).

3.2   Network Traffic Model

We consider a simplified version of the network traffic model studied in [10, 9, 11, 31, 32]. In this model at each time the network evolution is characterized by the following sequence of steps:

1. Each node produces a *data packet* at a given generation rate.

2. Each packet that is generated is assigned a destination, which is a randomly chosen node in the network.

3. Each node has a temporary memory (a *queue*) in which packets can be stored. When a node receives a packet it is placed at the bottom of its queue.

4. For each node that has at least one packet in its queue, the packet at the top of the queue is routed to one of its neighboring nodes.

5. The routing of packets depends on the queue length of the neighboring nodes. In what follows we make the assumption that the probability that a packet is routed to a certain node is inversely proportional to the node's queue length.

6. If two or more neighboring nodes are equally preferable for routing then a node will be chosen randomly.

7. If a packet reaches its target, it is removed from the queue of the destination node.

We assume, after time t the number of packets in the queue of node i be q_i^t and $q_i^t \neq 0$. Then at time $t+1$ the probability that node i sends one packet to node j is equal to,

$$\mathscr{P}_{ji}^{t+1} = \frac{A_{ji}\frac{1}{q_j^t}}{\sum\limits_{\ell}^{N} A_{\ell i}\frac{1}{q_\ell^t}} \tag{3.8}$$

We define the packet generation rate to be λ and the packet delivery rate to be μ_j. The packet delivery rate μ_j may not be same for all nodes. This is because even when nodes are equally likely to be selected as destinations for the packets, packets that are trying to reach certain destinations spend more time in the queues of the intermediary nodes than others, which decreases the effective delivery rate of those destinations. This can be seen from Table 4.1 that shows the average delivery rate (μ) numerically observed for the random ER graph in Fig.1.1(e) and $\lambda = 0.84$. Then, at time $t+1$ the queue length of node j will be equal to,

$$q_j^{t+1} = q_j^t + \sum_k^N A_{jk} \mathscr{P}_{jk}^t + \lambda - \mu_j - \Psi_j, \tag{3.9}$$

where Ψ_j is the number of packet routed by node j in a time step and is equal to either 0 or 1 (depending on whether there is at least one packet in the queue of node j or not). In the congested state, $\Psi_j = 1$ for all j's; then, by taking into account that the entries of the matrix A are either 0 or 1, Eq. (3.9) becomes,

$$q_j^{t+1} - q_j^t = \sum_k^N \frac{A_{jk}}{q_j^t \sum_\ell A_{\ell k} \frac{1}{q_\ell^t}} + \lambda - \mu_j - 1 \tag{3.10}$$

In simulation we observed the emergence of a congested state for which the queue lengths of the network nodes grow approximately linearly over time. Based on this observation, we introduce the assumption that, in the congested state, the queue length of node j can be written as $q_j^t \simeq \alpha_j t$, where α_j is the rate of growth of the queue length (*queue angle*) at node j. Then we can write,

$$q_j^{t+1} - q_j^t = \alpha_j = \sum_k^N \frac{A_{jk}}{\alpha_j t \sum_\ell A_{\ell k} \frac{1}{\alpha_\ell t}} + \lambda - \mu_j - 1 \tag{3.11}$$

$$\alpha_j^2 = \sum_k^N \frac{A_{jk}}{\sum_\ell A_{\ell k} \frac{1}{\alpha_\ell}} + \alpha_j(\lambda - \mu_j - 1) \tag{3.12}$$

By introducing the quantities $\tilde{\alpha}_i = \frac{1}{\alpha_i}$, we obtain,

$$\alpha_j^2 - \alpha_j(\lambda - \mu_j - 1) = \sum_k^N \frac{A_{jk}}{\sum_\ell^N A_{\ell k} \tilde{\alpha}_\ell} \tag{3.13}$$

The above equation can be re-written as,

$$\alpha_j(\alpha_j - \lambda + \mu_j + 1) = \sum_k^N \frac{A_{jk}}{\hat{\alpha}_k} \tag{3.14}$$

where, the vector $\hat{\alpha} = A^T \tilde{\alpha}$. By using a contraction mapping Eq. (3.14) can be solved iteratively in the unknown quantities α_j, that is, in the rates of growth at different nodes. In vector form we can write $\mathbf{Q}^t = \alpha t$, where $\mathbf{Q} = \{q_1, q_2, ..., q_N\}$ and $\alpha = \{\alpha_1, \alpha_2, ..., \alpha_N\}$.

3.3   Biological Excitable System

The Kinouchi and Copelli model [19] has been used to model the activity of a network of coupled biological excitable systems [33, 34, 35]. Each node i in the network is an excitable element and can be in one of $(m+1)$ states: $\kappa_i = 0$ is the resting state, $\kappa_i = 1$ corresponds to the excited state and the remaining $\kappa_i = 2, ..., m$ are refractory states, namely a state in which an excitable element is unable to receive or respond to an excitation. In each time-step an element (node) that is in resting state can become excited with a transition probability r (i.e. transition from $\kappa_i = 0$ to $\kappa_i = 1$) in two ways: either through an external excitation described by a Poisson process with probability η or with a probability A_{ij} for each neighbor j that was in the excited state in the previous time-step. Nodes in the excited and refractory state will transition deterministically into the next refractory state, if available, otherwise return to the resting state (Fig. 3.1).

The topology of the network is also described by the matrix $A = \{A_{ij}\}$, where we set $A_{ij} = A_{ji}$ to be equal to $0.5/K$ if node j can excite node i, otherwise $A_{ij} = 0$ and $K = N^{-1} \sum_{i,j} A_{ij}$ is the average node degree of the network. A node that is in the excited or
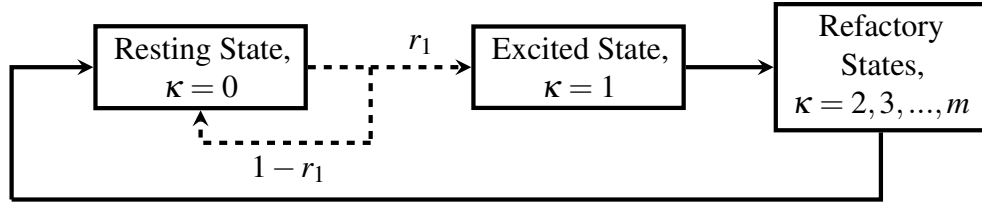
Figure 3.1: Schematic representation of the Kinouchi-Copelli Model

refractory state will deterministically transition into the next refractory state, until $\kappa_i = m$ after which it will transition again into the resting state $\kappa_i = 0$.

Using the analysis developed in Ref. [34] by Larremore. *et al.* we refer to Eq. (9) and Eq. (10) from [34] and write as the following.

$$p_i^{t+1} = \left(1 - \sum_{k=1}^{m} p_i^{t+1-k}\right)\left(\eta + (1-\eta)\left[1 - \prod_{j}^{N}\left(1 - A_{ij}p_j^t\right)\right]\right), \tag{3.15}$$

where p_i^t represents the probability that node i is excited at time t, m represents the number of refractory states (i.e. $\kappa = 0,1,2,...,m$) and η is the probability that a node is exited by an external stimulation. To understand Eq. (3.15), first note that a node can become excited at time $t+1$ only if it is in the susceptible state at time t, which explains the first term on the right hand side of Eq. (3.15). The second term on the right hand side of Eq. (3.15) represents the probability that a node that is susceptible at time t becomes excited, either via an external excitation described by the probability η or if at least one stimulus is received by one of the neighboring nodes (1 minus the probability that no stimulus is received). Note the underlying assumption of statistically independence. For more details, refer to Ref.[2, 30]. Following [34] by assuming that $A_{ij}p_j$ is small we replace $\prod_j^N \left(1 - A_{ij}p_j^t\right)$ by $\exp\left(-\sum_j^N A_{ij}p_j^t\right)$ and write,

$$p_i^{t+1} = \left(1 - \sum_{k=1}^{m_i} p_i^{t+1-k}\right)\left(\eta + (1-\eta)\left[1 - \exp\left(-\sum_{j}^{N} A_{ij}p_j^t\right)\right]\right) \tag{3.16}$$

and at steady state,

$$p_i = (1 - m_i p_i)\left(\eta + (1-\eta)\left[1 - \exp\left(-\sum_{j}^{N} A_{ij}p_j\right)\right]\right) \tag{3.17}$$

15

Chapter 4

Results

4.1 Evolutionary Game Theory

We numerically iterated the game on all the networks shown in Figs. 1.1 (a), (c) and (e) for a number of time-steps and for each node i we monitored $\langle S_i \rangle$ the fraction of times a node spends in the cooperator state. For each run, the game was iterated until a state was reached in which the number of cooperators and defectors did not change with time. Figs. 1.1(b) and 4.1 show the time fraction that each node spends in the cooperator state (results are averaged over both realization and time) for each one of the nodes of the network in Fig. 1.1(a), (c) and (e). Figure 4.1 presents the results of our numerical computations for the cases of the Bellsouth network in Fig. 1.1(c) and of the small random graph in Fig. 1.1(e). Note that in the figure the nodes are ordered by their degree. We observed that the nodes in the same cluster approximately show the same probability to be a cooperator (or defector) but that does not correlate with the degree. Here we see that the symmetries in the network topology plays a clear role on the resulting the dynamics more than the degree of the nodes.

(a)

(b)
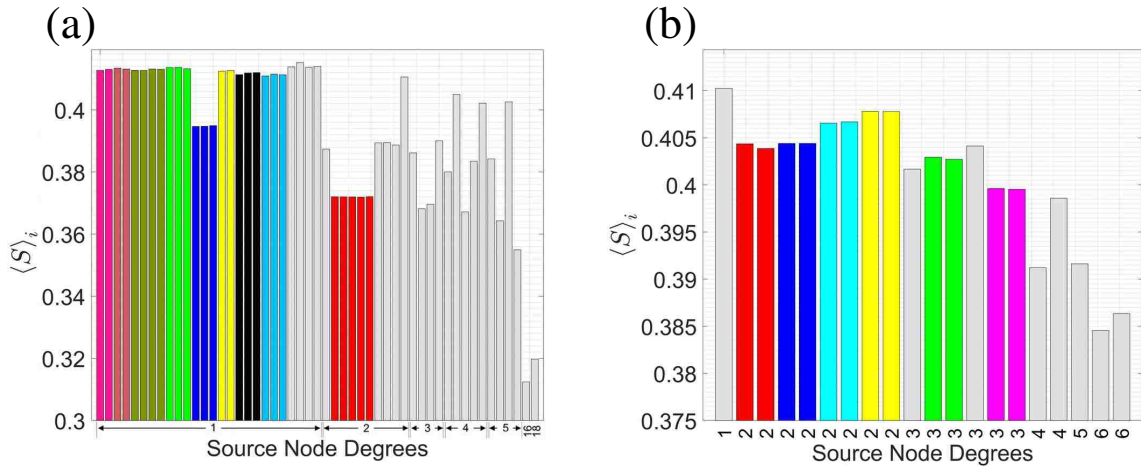
Figure 4.1: (a-b) Evolutionary game theory played on Bellsouth and random ER graph, see Fig. 1.1(b, c). Bars that are colored the same correspond to nodes in the same cluster (coloring is consistent with Fig. 1.1(b, c), the gray colored nodes, all of which are in a cluster by themselves.

4.2   Network Traffic Model

For this experiment, we set the generation rate to be equal to 0.84. That means in average 84% of nodes will generate a packet at each time step. Then, we have measured the queue angle of each node after a million of time-steps. Figures 1.1(d) and 4.2 show the outcome for the networks in Figs. 1.1(a), (c) and (e). For these networks, the nodes in the same clusters (as determined by the symmetry analysis) display similar queue lengths and delivery rate.

Table 4.1: Average delivery rate (μ) on the random ER graph shown in fig 1.1(c)

Node	μ	Node	μ	Node	μ	Node	μ
1	0.0928	6	0.2231	11	0.2325	16	0.0780
2	0.0688	7	0.1622	12	0.0829	17	0.1223
3	0.0682	8	0.1262	13	0.0626	18	0.0780
4	0.2207	9	0.1237	14	0.0622	19	0.1219
5	0.0327	10	0.1231	15	0.0840	20	0.0833
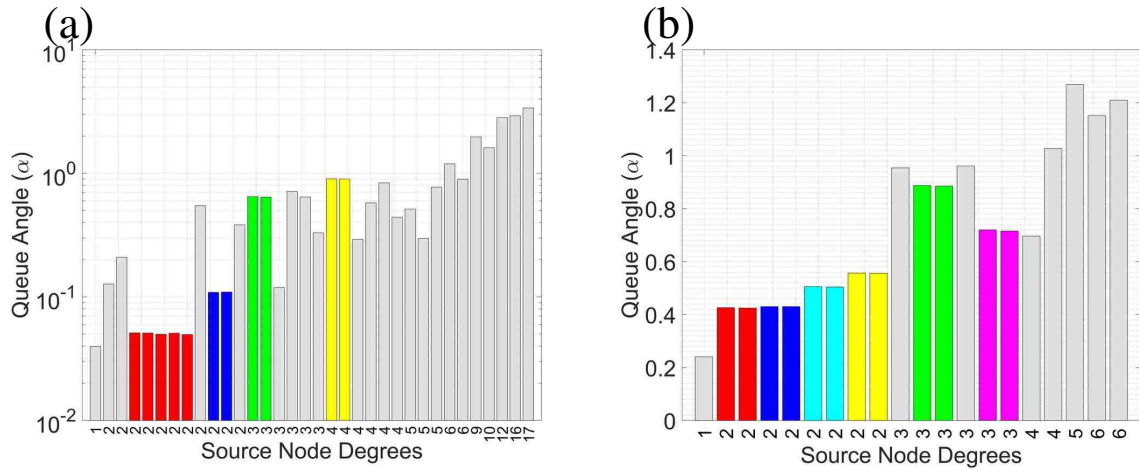
Figure 4.2: (a-b) Network traffic model simulated on Karate club and random ER graph, see Fig. 1.1(a, c).. Bars that are colored the same correspond to nodes in the same cluster (coloring is consistent with Fig. 1.1(a, c), the gray colored nodes, all of which are in a cluster by themselves.

4.3 Biological Excitable System

We numerically simulated the KC model on the networks shown in Figs. 1.1 (a), (c) and (e). We set $m = 6$, $\eta = 0.01$ and record the average time that each node spends in the excited state over a large number of time-steps. Figures 1.1(f) and 4.3 show the average node status (fraction of times a node spends in the excited state) after a million of time-steps for all three networks in Figs. 1.1. From these figures we see that, the effect of the network symmetries is apparent for the nodes that are in the same cluster.

It is easy to see that by removing the refractory period, the Kinouchi and Copelli model is mathematically equivalent to the classic SIS (susceptible-infected-susceptible) model used to model the spread of an epidemic in a population [12]. Indeed, our numerical investigations show the emergence of symmetries in the dynamics of the SIS model as well (not shown).

We have solved Eqs. (3.7), (3.14) and (3.17) iteratively in the steady-state and have

(a)

(b)
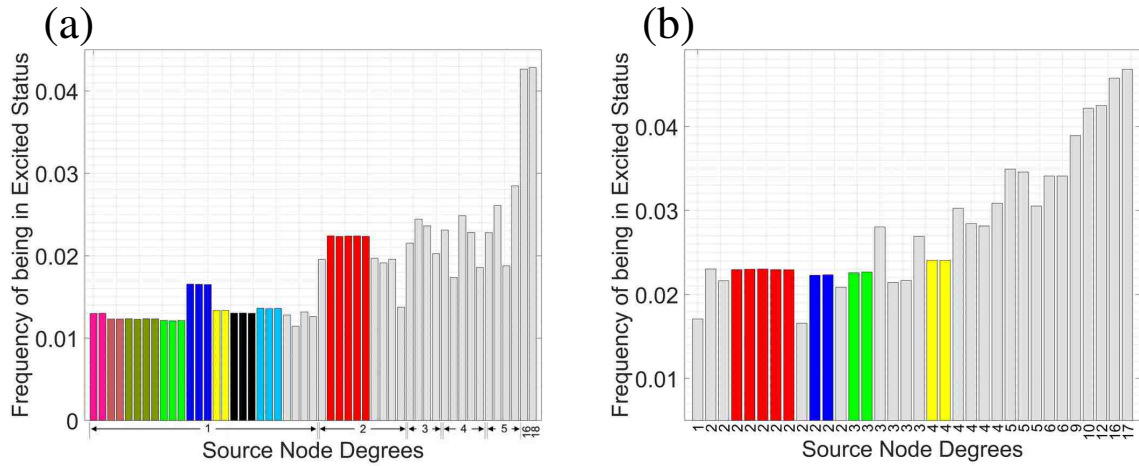
Figure 4.3: (a-b) Kinouchi Copelli model simulated on Bellsouth and Karate club network, see Fig. 1.1(a, b). Bars that are colored the same correspond to nodes in the same cluster (coloring is consistent with Fig. 1.1(a, b), the gray colored nodes, all of which are in a cluster by themselves.

shown the comparison between the iterative and full simulation results in Fig. 4.4. We see the analytic and simulation results are in good agreement between them. To conclude, the symmetry and clusters in the network topology play an important role. From the presence of symmetry and clusters, we can predict the possible contribution of the nodes in a cluster. This can reduce the computation effort significantly.
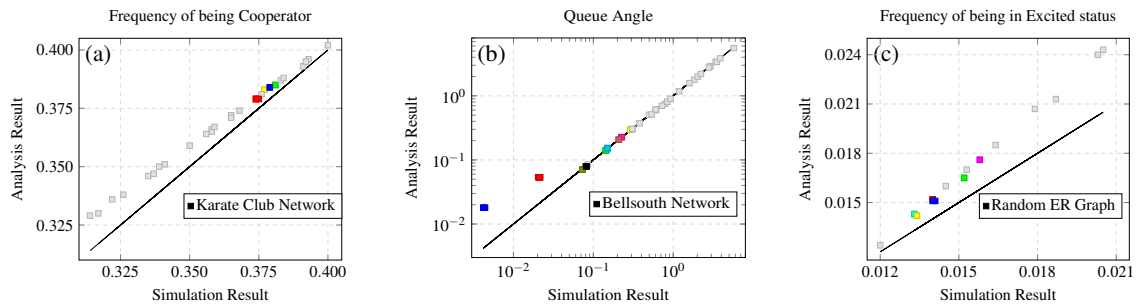
Figure 4.4: Each plot shows the comparison between the analytical results and the simulation results for one of the three dynamical scenarios. (a) shows the comparison for the case of evolutionary game theory results applied to the Karate club network, (b) shows the queue angle comparison for the network traffic model on Bellsouth Network and (c) represents the average node status comparison for the biological excitable system on Random ER network. Points that are colored the same correspond to nodes in the same cluster (coloring is consistent with Fig. 1.1, except for the gray colored nodes, each of which is in a cluster by itself.

Chapter 5

Symmetries and Stability Analysis

We analyzed each one of the three dynamical models that we have described above. We proved analytically that the equations admit solutions for which nodes that are swapped by a permutation matrix in the symmetry group maintain the same state indefinitely in time. We perturbed these particular solutions and analyze stability of each one of them. Just to provide some insight in how we proceeded, consider the mathematical description of the Kinouchi-Copelli model provided in Ref. [34, 36],

$$p_i^{t+1} = \left(1 - m p_i^t\right) \left(\eta + (1 - \eta) \left[1 - \exp\left(-\sum_j^N A_{ij} p_j^t \right) \right] \right), \tag{5.1}$$

$i = 1, ..., N$, where p_i^t is the probability that node i is in the excited state at time t and here we assume $m = 6$. By considering the vector $\mathbf{p}^t = [p_1^t, p_2^t, ..., p_N^t]$ and premultiplying the vectorial version of Eq. (5.1) by $\Pi \in \mathscr{G}$, we see that Eqs. (5.1) admit a solution where nodes that are symmetric maintain the same value of p_i^t over time. By applying a small perturbation, it will then be possible to ascertain whether this particular solution is stable or unstable.

5.1   Evolutionary Game Theory

We are now looking for the effect of the network symmetries on the dynamics. Our goal is to prove that Eq. (3.7) is equivariant under permutations of the network nodes that are in the automorphism group of A. We look at Eq. (3.7) and consider symmetries(Π) of A, that is, Π is a permutation matrix such that $\Pi A = A\Pi$. Our goal is to prove that if $\Pi \langle \mathbf{S} \rangle^t = \langle \mathbf{S} \rangle^t$, then $\Pi \langle \mathbf{S} \rangle^{t+1} = \langle \mathbf{S} \rangle^{t+1}$. To this end it is sufficient to observe that $\Pi \langle \mathbf{F} \rangle = \langle \mathbf{F} \rangle$, $\Pi \langle \mathbf{F_C} \rangle = \langle \mathbf{F_C} \rangle$ and $\Pi \boldsymbol{\sigma} (\langle \mathbf{x} \rangle) = \boldsymbol{\sigma} (\langle \mathbf{x} \rangle)$.

Let's first apply the permutation matrix Π to $\boldsymbol{\sigma} (\langle \mathbf{x} \rangle)$. Then,

$$\Pi \boldsymbol{\sigma} (\langle \mathbf{x} \rangle) = \Pi \boldsymbol{\sigma} (2 \langle \mathbf{F_C} \rangle - \langle \mathbf{F} \rangle) = 2\gamma \Pi \langle \mathbf{F_C} \rangle - \gamma \Pi \langle \mathbf{F} \rangle + \varepsilon$$

Now if we can show that $\Pi \langle \mathbf{F} \rangle = \langle \mathbf{F} \rangle$ and $\Pi \langle \mathbf{F_C} \rangle = \langle \mathbf{F_C} \rangle$, then we see that $\Pi \boldsymbol{\sigma} (\langle \mathbf{x} \rangle) = \boldsymbol{\sigma} (\langle \mathbf{x} \rangle)$.

We write the payoff vector, $\boldsymbol{\xi} = bA^T \mathbf{S} - c\Omega \mathbf{S} = (bA^T - c\Omega) \mathbf{S}$, where Ω is a diagonal matrix such that $\Omega_{ii} = \sum_j^N A_{ij}$. Then from Eqns. (3.5) and (3.6) we write the vector form of $\langle \mathbf{F} \rangle$ and $\langle \mathbf{F_C} \rangle$,

$$\langle \mathbf{F} \rangle = A \left[1 - \omega + \omega \left(bA^T - cK \right) \langle \mathbf{S} \rangle \right]$$
$$\langle \mathbf{F_C} \rangle = A \left[\langle \mathbf{S} \rangle \circ \left(1 - \omega + \omega \left(bA^T - cK \right) \langle \mathbf{S} \rangle \right) \right],$$

(5.2)

where, the symbol "$\circ$" represents the "Hadamard Product". Applying the permutation matrix Π to $\langle \mathbf{F} \rangle$. Then,

$$\Pi \langle \mathbf{F} \rangle = A\Pi \left[1 - \omega + \omega (bA^T - cK) \langle \mathbf{S} \rangle \right] = A \left[1 - \omega + \omega (bA^T - cK)\Pi \langle \mathbf{S} \rangle \right] = \langle \mathbf{F} \rangle$$

We note that nodes that are symmetric to each other have also the same degree. Thus from the definition of the matrix Ω it follows that $\Pi \Omega = \Omega \Pi$. We can also show that $\Pi A^T = \Pi^T A^T = (A\Pi)^T = (\Pi A)^T = A^T \Pi^T = A^T \Pi$. Similarly we can write, $\Pi \langle \mathbf{F_C} \rangle = \langle \mathbf{F_C} \rangle$. Therefore,

$$\Pi \langle \mathbf{S} \rangle^{t+1} = \frac{N-1}{N} \Pi \langle \mathbf{S} \rangle^t + \frac{1}{N} \Pi \boldsymbol{\sigma} (\langle \mathbf{x} \rangle) = \frac{N-1}{N} \langle \mathbf{S} \rangle^t + \frac{1}{N} \boldsymbol{\sigma} (\langle \mathbf{x} \rangle) = \langle \mathbf{S} \rangle^{t+1}$$

We see that Eq. (3.7) can be solved iteratively at steady state in the unknown quantities $\langle \mathbf{S} \rangle_i$, $i = 1, 2, ..., N$. This is shown in Fig. 4.4(a) where $\langle \mathbf{S} \rangle_i$ obtained by the iterative solution of Eq. (3.7) at steady state is plotted versus the value of $\langle \mathbf{S} \rangle_i$ obtained from the numerical simulation of the game averaged over a number of realizations colors are consistent with Fig. 1.1(a).

Now we want to find the stability of a fixed point solution for Eq. (3.7). We linearize Eq. (3.7) about fixed point $\langle \bar{\mathbf{S}} \rangle$,

$$\delta \langle \mathbf{S} \rangle^{t+1} = \frac{N-1}{N} \delta \langle \mathbf{S} \rangle^t + \frac{\gamma}{N} \delta \langle \mathbf{x} \rangle, \tag{5.3}$$

which is the same as,

$$\delta \langle \mathbf{S} \rangle^{t+1} = \frac{N-1}{N} \delta \langle \mathbf{S} \rangle^t + \frac{2\gamma}{N} \delta \langle \mathbf{F_C} \rangle - \frac{\gamma}{N} \delta \langle \mathbf{F} \rangle \tag{5.4}$$

and we can write,

$$\delta \langle \mathbf{S} \rangle^{t+1} = \left[\frac{N-1}{N} - \frac{\gamma}{N} A \omega \left(bA^T - c\Omega \right) \right] \delta \langle \mathbf{S} \rangle^t + \frac{2\gamma}{N} \delta \langle \mathbf{F_C} \rangle \tag{5.5}$$

and finally we get,

$$\delta \langle \mathbf{S} \rangle^{t+1} = \left[\frac{N-1}{N} - \frac{\gamma}{N} AD + \frac{2\gamma}{N} M_{\langle \bar{\mathbf{S}} \rangle} \right] \delta \langle \mathbf{S} \rangle^t, \tag{5.6}$$

where the matrices, $M_{\langle \bar{\mathbf{S}} \rangle} = diag(\langle \bar{\mathbf{S}} \rangle)D + diag(D\langle \bar{\mathbf{S}} \rangle + 1 - \omega)$ and $D = \omega \left(bA^T - c\Omega \right)$.

5.2   Network Traffic Model

As before, assume that Π is a permutation of A. We want to show that if $\Pi \mathbf{Q}^t = \mathbf{Q}^t$, then $\Pi \mathbf{Q}^{t+1} = \mathbf{Q}^{t+1}$, assume $\Pi \mathbf{Q}^t = \mathbf{Q}^t \Pi$. We will now try to prove $\Pi \mathbf{Q}^{t+1} = \mathbf{Q}^{t+1}$ from Eq. (3.10) without using the ansatz $q_j^t = \alpha_j^t t$. We can rewrite Eq. (3.10) in vector form,

$$\mathbf{Q}^{t+1} = \mathbf{Q}^t + A^T \left(1 \circ^{-1} \left(A^T \left(1 \circ^{-1} \mathbf{Q}^t \right) \right) \right) \circ \left(1 \circ^{-1} \mathbf{Q}^t \right) + \lambda - \mu - 1 \tag{5.7}$$

Where, the symbol "$1 \circ^{-1}$" represents the Hadamard division, i.e., multiplication with the inverse elements of the matrix or vector. We pre-multiply both sides of Eq. (5.7) by Π and obtain,

$$\Pi \mathbf{Q}^{t+1} = \Pi \mathbf{Q}^t + \Pi A^T \left(1 \circ^{-1} \left(A^T \left(1 \circ^{-1} \mathbf{Q}^t \right) \right) \right) \circ \Pi \left(1 \circ^{-1} \mathbf{Q}^t \right) + \lambda - \mu - 1 =$$

$$\mathbf{Q}^t + A^T \left(1 \circ^{-1} \left(\Pi A^T \left(1 \circ^{-1} \mathbf{Q}^t \right) \right) \right) \circ \left(1 \circ^{-1} \Pi \mathbf{Q}^t \right) + \lambda - \mu - 1 =$$

$$\mathbf{Q}^t + A^T \left(1 \circ^{-1} \left(A^T \Pi \left(1 \circ^{-1} \mathbf{Q}^t \right) \right) \right) \circ \left(1 \circ^{-1} \mathbf{Q}^t \right) + \lambda - \mu - 1 =$$

$$\mathbf{Q}^t + A^T \left(1 \circ^{-1} \left(A^T \left(1 \circ^{-1} \Pi \mathbf{Q}^t \right) \right) \right) \circ \left(1 \circ^{-1} \mathbf{Q}^t \right) + \lambda - \mu - 1 =$$

$$\mathbf{Q}^t + A^T \left(1 \circ^{-1} \left(A^T \left(1 \circ^{-1} \mathbf{Q}^t \right) \right) \right) \circ \left(1 \circ^{-1} \mathbf{Q}^t \right) + \lambda - \mu - 1 = \mathbf{Q}^{t+1}$$

Another way to prove the same result is by using our ansatz $q_j^t = \alpha_j^t$, which holds for the congested state. Then it follows immediately that $\Pi \alpha = \alpha$ and that $\Pi \mathbf{Q}^{t+1} = \mathbf{Q}^{t+1}$.

Adding small perturbations, from eq. 3.10 we see that the perturbations δq_j^t obey the following equation,

$$\delta \dot{q}_j = -\sum_k^N \frac{A_{jk}}{q_j^2 \hat{\alpha}_k} \delta q_j + \frac{1}{q_j} \sum_k^N A_{jk} \frac{1}{\hat{\alpha}_k^2} \sum_\ell^N A_{\ell k} \frac{1}{q_\ell^2} \delta q_\ell \tag{5.8}$$

And finally we can write,

$$\dot{\delta \mathbf{q}} = \Xi \delta \mathbf{q} \tag{5.9}$$

where, $\delta \mathbf{q} = [\delta q_1, \delta q_2, ..., \delta q_N]$ and the entries of the matrix Ξ, $\Xi_{ij} = \frac{1}{q_i q_j^2} \sum_\ell^N A_{i\ell} \frac{1}{\hat{\alpha}_\ell^2} A_{j\ell} - \delta_{ij} \sum_\ell^N \frac{A_{i\ell}}{q_i^2 \hat{\alpha}_\ell}$ and δ_{jl} is the Kronecker delta.

5.3   Biological excitable system

We also want to analyze the effect of symmetry in the biological excitable system [19], [34]. To this end, we write the vector versions of Eq.(3.16) and Eq.(3.17),

$$\mathbf{P}^{t+1} = \left(1 - \sum_{k=1}^{m} \mathbf{P}^{t+1-k}\right) \circ \left(\eta + (1-\eta)\left[1 - \exp\left(-A\mathbf{P}^t\right)\right]\right) \tag{5.10}$$

and for the steady state,

$$\mathbf{P} = (1 - m\mathbf{P}) \circ \left(\eta + (1-\eta)\left[1 - \exp\left(-A\mathbf{P}\right)\right]\right) \tag{5.11}$$

We look at Eq. (5.10) and consider symmetries(Π) of A, that is permutation matrices such that $\Pi A = A\Pi$. Again, we assume that Π permutes with $\mathbf{P}^t, \mathbf{P}^{t-1}, ..., \mathbf{P}^{t-m+1}$ then we want to show that Π also permutes with $\mathbf{P}^{t+1}$. Let's premultiply by Π both sides of the Eq. (5.10) and we write,

$$\Pi\mathbf{P}^{t+1} = \Pi\left(\left(1 - \sum_{k=1}^{m_i} \mathbf{P}^{t+1-k}\right) \circ \left(\eta + (1-\eta)\left[1 - \exp\left(-A\mathbf{P}^t\right)\right]\right)\right) =$$

$$\Pi\left(1 - \sum_{k=1}^{m_i} \mathbf{P}^{t+1-k}\right) \circ \Pi\left(\eta + (1-\eta)\left[1 - \exp\left(-A\mathbf{P}^t\right)\right]\right) =$$

$$\left(1 - \Pi\sum_{k=1}^{m_i} \mathbf{P}^{t+1-k}\right) \circ \left(\eta + (1-\eta)\left[1 - \exp\left(-\Pi A\mathbf{P}^t\right)\right]\right) =$$

$$\left(1 - \left(\Pi\mathbf{P}^t + \Pi\mathbf{P}^{t-1} + ... + \Pi\mathbf{P}^{t-m+1}\right)\right) \circ \left(\eta + (1-\eta)\left[1 - \exp\left(-A\Pi\mathbf{P}^t\right)\right]\right) =$$

$$\left(1 - \left(\mathbf{P}^t + \mathbf{P}^{t-1} + ... + \mathbf{P}^{t-m+1}\right)\right) \circ \left(\eta + (1-\eta)\left[1 - \exp\left(-A\mathbf{P}^t\right)\right]\right) =$$

$$\left(1 - \sum_{k=1}^{m_i} \mathbf{P}^{t+1-k}\right) \circ \left(\eta + (1-\eta)\left[1 - \exp\left(-A\mathbf{P}^t\right)\right]\right) = \mathbf{P}^{t+1}$$

We note that Eq. (5.11) can be iteratively solved in the unknown quantities $P_1, P_2, ..., P_N$. This is shown in Fig. 4.4(c) where we plotted the average status of a node from iteration of Eq. 5.11 versus the average time that it is found in the excited state from the full simulation of the Kinouchi and Copelli model [19].

To analyze stability of the solution, following Ref.[36] we linearize Eq. (5.10) around the quiescent fixed point $\mathbf{P} = \mathbf{0}$,

$$\delta P^{t+1} = (1 - m\bar{\mathbf{P}}) \circ (1 - \eta) A \exp(-A\bar{\mathbf{P}}) \delta P(t) \tag{5.12}$$

when there is no external excitation i.e. $\eta = 0$, we can write Eq. (5.12)

$$\delta P^{t+1} = A \delta P(t) \tag{5.13}$$

The result of the stability analysis will extend to the case of $\eta > 0$, because here η plays the role of an external input.

Chapter 6

Quotient Graph Reduction

6.1 Quotient Graph

As mentioned in the introduction, symmetries are common features of real networks. For example biological network, technological network, social network etc. We have displayed a short table for these networks and the data were collected from the article [20] by *MacArthur. et al.*

Table 6.1: No of symmetries in some real world networks [20]

Network	No of nodes	No of edges	No of symmetries
Human B Cell Genetic (BCell) [37]	$5,390$	$64,645$	5.9374×10^{13}
Internet (AS Level) (IntAS) [38]	$22,332$	$45,392$	1.2822×10^{11298}
US Power Grid (USPow) [39]	$4,941$	$6,594$	5.1851×10^{152}
US Airports (USAir) [40]	332	$2,126$	2.5916×10^{24}
PhD network (PhD) [41]	$1,025$	$1,043$	2.9810×10^{292}
PGP users network (PGP) [42]	$10,680$	$24,316$	4.4963×10^{1251}

Intensive research in social sciences, biology, engineering and physics attempts to use numerical simulations of large dynamical networks to understand and predict their behavior,

often with the goal of better characterizing and understanding of real world phenomena.

Our results in Secs. II and III point out that nodes that are symmetric to each other often display the same average behavior (if the cluster state is stable). This immediately raises the question whether a reduction of the dynamics is possible in which *duplicate nodes* can be omitted, which would be helpful in reducing the computational complexity of simulations of large complex networks. Indeed, we know that in the case of synchronizaion, a *quotient network reduction* is possible, in which the exact cluster-synchronous time evolution of the nodes can be generated by a reduced number of nodes, equal to the number of clusters (i.e., a node for each cluster).

Here we explain how the quotient network can be obtained. A graph is an ordered pair $G = (V, E)$ consisting of a nonempty vertex set V of vertices $(n(V) = N)$ and edge set E of edges and automorphism permutes the vertices $(v \subset V)$ preserving the adjacency and non-adjacency of the graph or network. The set of all automorphisms of a graph form a group called the Automorphism Group written as $Aut(G)$. We can say under the action of $\mathcal{G} = Aut(G)$ the vertex set $V(G)$ is partitioned into C disjoint structural equivalence classes called *G-orbits* of v such that

$$\mathcal{O}_{\mathcal{G}}(v) = \{u \in V | \exists g \in \mathcal{G} \text{ such that } gv = u\}$$

$$\bigcup_{\ell=1}^{C} n\left(\mathcal{O}_{\mathcal{G}}^{\ell}\right) = N \text{ and } \mathcal{O}_{\mathcal{G}}^{i} \cap \mathcal{O}_{\mathcal{G}}^{j} = 0, \text{ where } i, j = 1, 2, ..., C, j \neq i$$

The nodes or vertices of an orbit hold the equivalence relation $\sim$, The quotient graph of G with respect to $\sim$ is a graph $\mathcal{Q}_G$ such that its vertex set is the quotient set $V / \sim$ and two equivalence classes $[u]$, $[v]$ form an edge iff uv forms an edge in $\mathcal{G}$. Graphs in Figs. 6.3 and 6.7 are the quotient graphs of the graphs in Figs. 6.2 and 6.6. If $\mathcal{O}^v, \mathcal{O}^u$ are any two orbits or equivalence classes of the group $\mathcal{G}$, then we can write the expression of the quotient graph $\mathcal{Q}_G$ of graph G such that for each pair of sets $(\mathcal{O}^v, \mathcal{O}^u)$,

$$\mathcal{Q}_{uv} = \frac{1}{n(\mathcal{O}^u)} \sum_{i \in \mathcal{O}^u} \sum_{j \in \mathcal{O}^v} A_{ij},$$
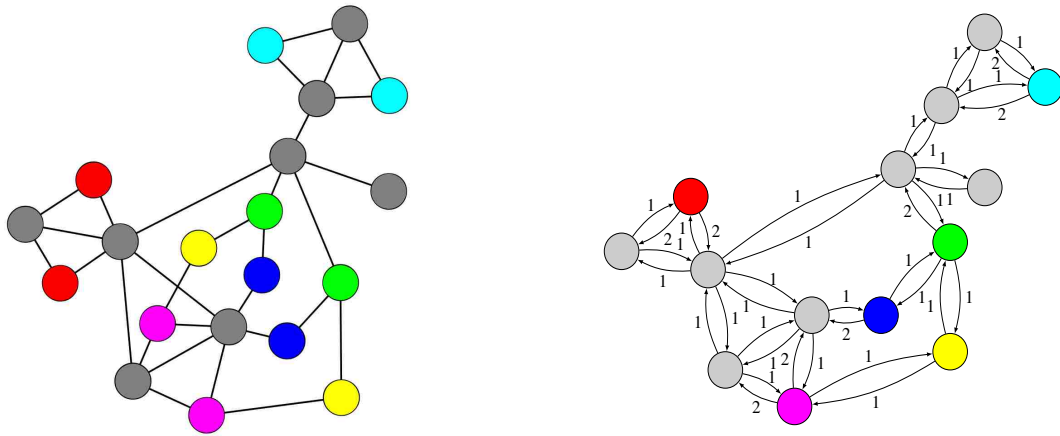
Figure 6.1: The Random ER graph and its quotient graph reduction

where $u, v = 1, 2, ..., C$. In Fig. 6.1 we demonstrate an example of quotient graph reduction from if's full graph shown in Fig. 1.1(e), where we can see the nodes in the same orbit are reduced to one node and the corresponding color identifies each reduced node.

6.2 Quotient Graph Analogy

We envision that the quotient graph of a network could be an conveniently exploited in simulations involving large networks to reduce their computational complexity. These simulations may be used to study epidemics, congestion, emergence of cooperation, as discussed in Chapter. III - V, just to mention a few examples. In order to demonstrate the potential usefulness of an equivalent model on the quotient network, we choose to work with the Kinouchi Copelli model. For a number of networks, we use their quotient graph reductions to study how well they can approximate the full Kinouchi Copelli dynamics of the original network.

We start by considering a simple network of five nodes shown in Fig. 6.2 with two nontrivial clusters and one trivial cluster. The mathematical equations we have derived in

Chapter. III for all the three models can be easily projected on to the corresponding quotient network equations. However coming up with an equivalent model that can be simulated on the quotient network may require a particular adaptation of the model, which is model specific. To show this last point we consider the particular case of the Kinouchi Copelli model, which we describe in detail in what follows.

$$A = \begin{bmatrix} 0 & \beta & 0 & 0 & 0 \\ \beta & 0 & \beta & 0 & 0 \\ 0 & \beta & 0 & \beta & 0 \\ 0 & 0 & \beta & 0 & \beta \\ 0 & 0 & 0 & \beta & 0 \end{bmatrix}$$

Figure 6.2: 5 Nodes Network. Colors distinguish the orbits of the automorphism group. The matrix A on the right describes the adjacency of the network

From (3.15) for the network presented in Fig. 6.2 we can write,

$$p_1^{t+1} = \left(1 - \sum_{k=1}^{m} p_1^{t+1-k}\right) \left(\eta + (1-\eta)\beta p_2^t\right) \tag{6.1}$$

$$p_2^{t+1} = \left(1 - \sum_{k=1}^{m} p_2^{t+1-k}\right) \left(\eta + (1-\eta)\left[1 - (1-\beta p_1^t)(1-\beta p_3^t)\right]\right) \tag{6.2}$$

$$p_3^{t+1} = \left(1 - \sum_{k=1}^{m} p_3^{t+1-k}\right) \left(\eta + (1-\eta)\left[1 - (1-\beta p_2^t)(1-\beta p_4^t)\right]\right) \tag{6.3}$$

$$p_4^{t+1} = \left(1 - \sum_{k=1}^{m} p_4^{t+1-k}\right) \left(\eta + (1-\eta)\left[1 - (1-\beta p_3^t)(1-\beta p_5^t)\right]\right) \tag{6.4}$$

$$p_5^{t+1} = \left(1 - \sum_{k=1}^{m} p_5^{t+1-k}\right) \left(\eta + (1-\eta)\beta p_4^t\right) \tag{6.5}$$

We define the cluster state, where $y_1^t = p_1^t = p_5^t$, $y_2^t = p_2^t = p_4^t$ and $y_3^t = p_3^t$. So we can rewrite Eqs. (6.3), (6.4) and (6.5) in the new y-coordinate system as,

$$y_1^{t+1} = \left(1 - \sum_{k=1}^{m} y_1^{t+1-k}\right)\left(\eta + (1-\eta)\beta y_2^t\right) \tag{6.6}$$

$$y_2^{t+1} = \left(1 - \sum_{k=1}^{m} y_2^{t+1-k}\right)\left(\eta + (1-\eta)\left[1 - (1 - \beta y_1^t)(1 - \beta y_3^t)\right]\right) \tag{6.7}$$

$$y_3^{t+1} = \left(1 - \sum_{k=1}^{m} y_3^{t+1-k}\right)\left(\eta + (1-\eta)2\beta y_2^t\right) \tag{6.8}$$

From the eqs. (6.6), (6.7) and (6.8) we can build the reduced matrix B shown in figure 6.3, which coincides the quotient graph obtained from the full network A.
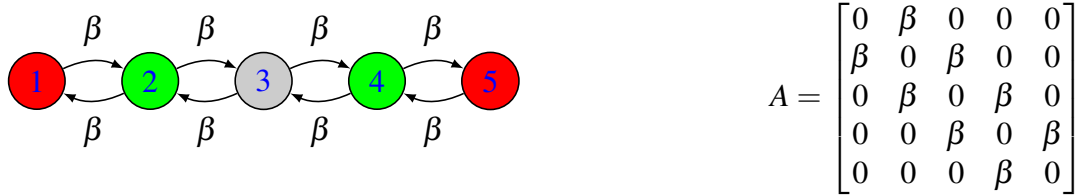

Figure 6.3: Quotient graph of the 5 Nodes Network 6.2. Colors distinguish the orbits of the automorphism group. The matrix B on the right describes the quotient network.

We verified this fact with the iterative solution of the problem as well. We also applied this quotient graph reduction for the network in Fig. 6.2 to the other dynamical models and found it matched pretty well with the full graph results.

6.3 Simulation with network quotients

We applied the network quotients in the simulations of different dynamical models. Due to some incompatibility between the network quotient structure and the philosophy of the

model, some simulations on the quotient graphs needed to rescale to compare with the result of full network simulations. For example we have accomplished the simulation of Kinouchi Copelli Model on several simple networks shown in Figs. (6.2 - 6.5) and tabulated the results in table 6.2.

$$A = \begin{bmatrix} 0 & \beta & 0 & 0 & 0 & 0 \\ \beta & 0 & \beta & 0 & 0 & 0 \\ 0 & \beta & 0 & \beta & 0 & 0 \\ 0 & 0 & \beta & 0 & \beta & 0 \\ 0 & 0 & 0 & \beta & 0 & \beta \\ 0 & 0 & 0 & 0 & \beta & 0 \end{bmatrix}$$

Figure 6.4: Simple 6 Nodes Network. Colors distinguish the orbits of the automorphism group. The matrix *A* on the right describes the adjacency of the network

$$B = \begin{bmatrix} 0 & \beta & 0 \\ \beta & 0 & \beta \\ 0 & \beta & \beta \end{bmatrix}$$

Figure 6.5: Quotient graph of the 6 Nodes Network 6.4. Colors distinguish the orbits of the automorphism group. The matrix *B* on the right describes the connectivity of the network.

Table 6.2: Comparison between full and quotient graph

5-Nodes Network				6-Nodes Network			
Full		Quotient		Full		Quotient	
Node	p_i	Node	p_i	Node	p_i	Node	p_i
1	0.0112	1	0.0110	1	0.0112	1	0.0111
2	0.0127	2	0.0122	2	0.0127	2	0.0124
3	0.0129	3	0.0129	3	0.0129	3	0.0112
4	0.0126			4	0.0128		
5	0.0112			5	0.0126		
				6	0.0112		

Refer to table 6.2, when we compared the outcomes of simulations of Kinouchi Copelli

model done on the network in fig 6.6 and its quotient graph 6.7 we needed to rescale the outcome because of the presence of self loop in the quotient graph.

This self-loop describes the probability of that node to be excited by itself but as per the dynamical scenario a node cannot excite it-self. So the effect of self-loop is ignored in the simulation. Since we ignored the self-loop in our simulation, we lost the contribution of that probability in the simulation. This is why we needed to adjust the outcomes making some projections. In this case we made a suitable projection function like eq. (6.9) and was able to achieve the result close to the results of full simulation. We extend the results for simple 9 nodes network shown in Fig. 6.6 and its quotient shown in Fig. 6.7. We presented the result after the scaling in table 6.3.

$$q_i^f = \left(1 - \frac{n_i}{m} - q_i n_i\right) q_i \tag{6.9}$$

where, q_i^f represents the outcome after the projection of q_i and n_i represents the number of self connections in the orbit of node i.

$$B = \begin{bmatrix} 0 & \beta & 0 & 0 & 0 & 0 & 0 & 0 & 0 \\ \beta & 0 & \beta & 0 & 0 & 0 & 0 & 0 & 0 \\ 0 & \beta & 0 & \beta & \beta & 0 & 0 & 0 & 0 \\ 0 & 0 & \beta & 0 & \beta & \beta & 0 & 0 & 0 \\ 0 & 0 & \beta & \beta & 0 & 0 & 0 & \beta & 0 \\ 0 & 0 & 0 & \beta & 0 & 0 & \beta & 0 & 0 \\ 0 & 0 & 0 & 0 & 0 & \beta & 0 & 0 & 0 \\ 0 & 0 & 0 & 0 & \beta & 0 & 0 & 0 & \beta \\ 0 & 0 & 0 & 0 & 0 & 0 & 0 & \beta & 0 \end{bmatrix}$$
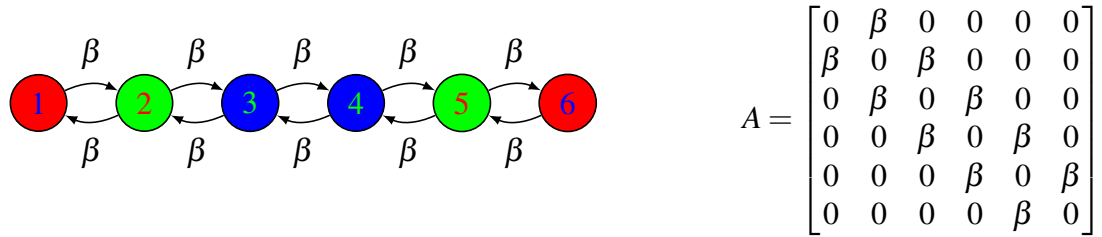
Figure 6.6: Simple 9 Nodes Network. Colors distinguish the orbits of the automorphism group. The matrix *A* on the right describes the adjacency of the network
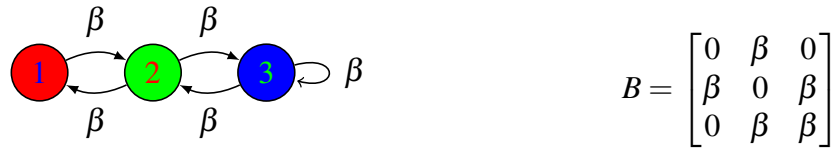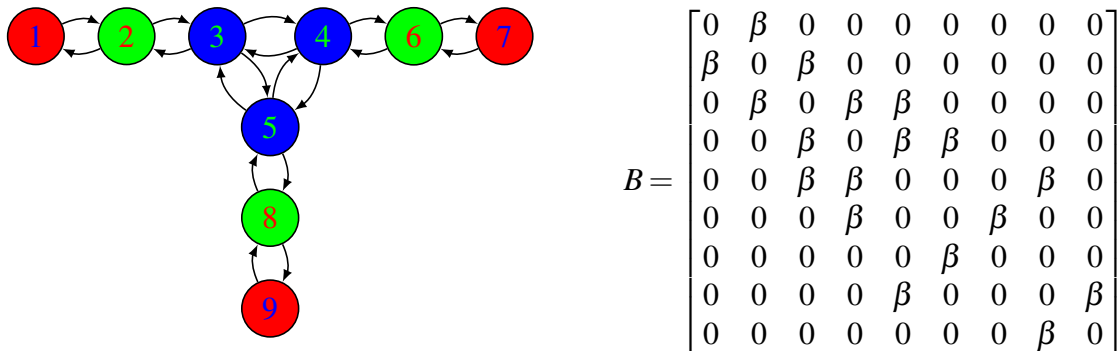
Figure 6.7: Quotient graph of the 9 Nodes Network 6.6. Colors distinguish the orbits of the automorphism group. The matrix B on the right describes the connectivity of the network.

Table 6.3: Comparison between full and quotient graph

9-Nodes Network				6-Nodes Network			
Full		Quotient		Full		Quotient	
Node	p_i	Node	p_i	Node	p_i	Node	p_i
1	0.0110	1	0.0108	1	0.0112	1	0.0111
2	0.0123	2	0.0119	2	0.0127	2	0.0124
3	0.0140	3	0.0144	3	0.0129	3	0.0129
4	0.0139			4	0.0128		
5	0.0143			5	0.0126		
6	0.0123			6	0.0112		
7	0.0109						
8	0.0122						
9	0.0109						

6.4 Modification of the Model

To overcome the limitations in simulation with quotient graph we modified the Knouchi Copelli model. To incorporate the self-loop excitation of quotient graph we introduced a second transition probability r_2 to go to the refractory state from the excited state as shown in figure 6.8. The transition probability r_{2j} will depend on number of self-loop present in node j. If there is no self-loop present in node j then $r_{2j} = 1$, other wise r_{2j} will depend on the self-loop present in the nodes. This is how for no self-loop the modified model converges with the original model.

We have done the simulations with quotient graphs based on the dynamics of modified Kinouchi Copelli model on the simple networks shown in Figs. (6.4-6.7) and tabulated in
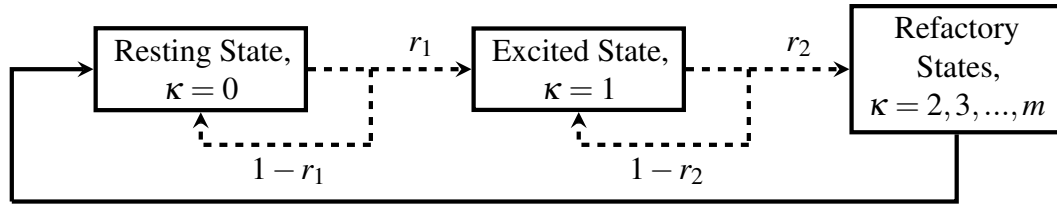
Figure 6.8: Schematic representation of the modified Kinouchi-Copelli Model

table 6.4 to compare the results with the full graphs and achieve good matching with the simulations done on the full networks.

Table 6.4: Comparison between full and quotient graph

9-Nodes Network				6-Nodes Network			
Full		Quotient		Full		Quotient	
Node	p_i	Node	p_i	Node	p_i	Node	p_i
1	0.0110	1	0.0109	1	0.0112	1	0.0112
2	0.0123	2	0.0123	2	0.0127	2	0.0126
3	0.0140	3	0.0140	3	0.0129	3	0.0128
4	0.0139			4	0.0128		
5	0.0143			5	0.0126		
6	0.0123			6	0.0112		
7	0.0109						
8	0.0122						
9	0.0109						

At this point we can conclude saying that, to solve a dynamical scenario iteratively, its quotient graph can reduce the computational effort to produce the same solution and depending upon the topology of any network a suitable projection of results of quotient graph can lead to a good consensus of the results with full network simulation.

Chapter 7

Discussion

7.1 Summary

Symmetry is evident is almost everywhere form a mechanical structure to biological organism. In our everyday life we can see a lot of examples of the presence of symmetry i.e. crystal structure of a molecule, HiV virus, flowers etc. For this reason my study of symmetries in dynamical networks is very significant in light of network redundancy and computational complexity. Specially in the large networks the computational complexity becomes really a great problem so if we can reduce our network to a smaller one based on the topological symmetries that will reduce the computational complexity significantly. In my current I tried to show the effect of topological symmetry in the outcomes of the simulation of various dynamical models and eventually show a matching of results between the full network and its quotient reduction.

HIV virus　　　　　　　　　　　　　　　　　　　**Lilium**
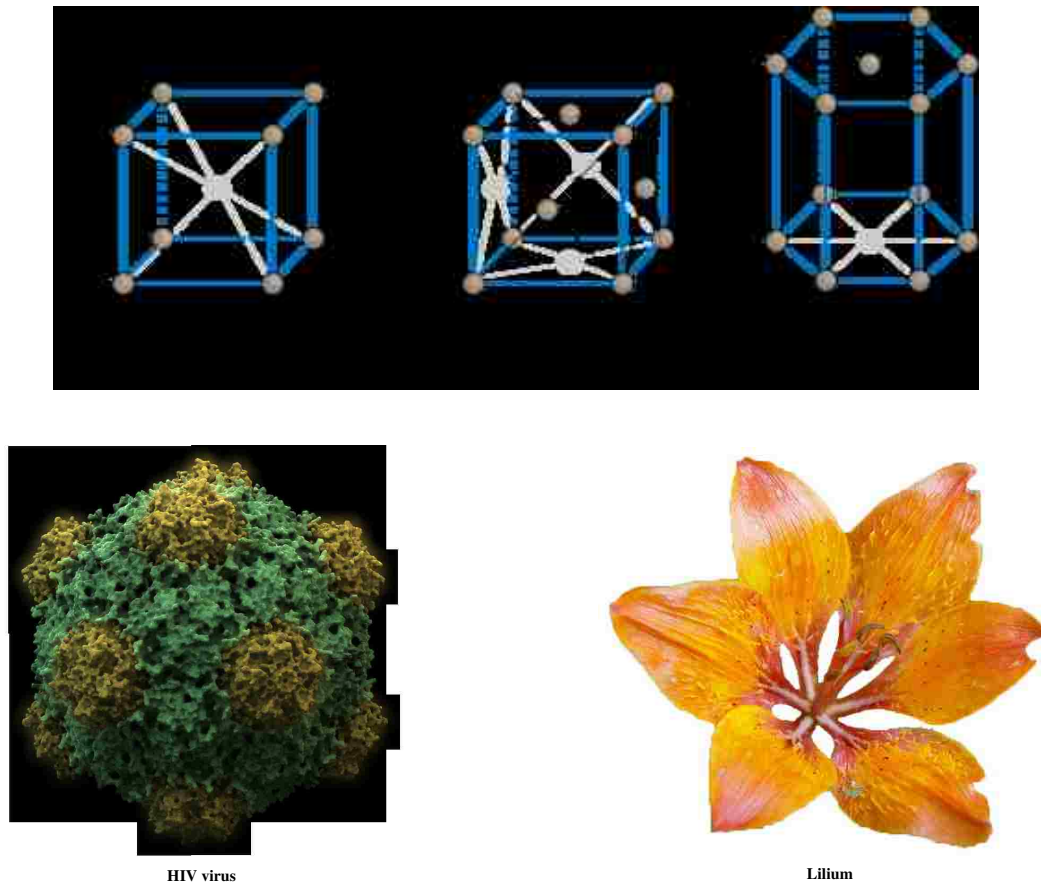
Figure 7.1: Symmetries in everyday life

7.1.1 Methodology

For the current study I have done the numerical simulations of various dynamical models for several real and randomly generated networks using MATLAB. To identify the network symmetries I adopted the computational graph theory and in this regard I used an open source software named SAGE. Because sometimes for larger network it becomes quite impossible to identify the underlying symmetries of the networks only my inspection. Since for my study it is important to find the symmetries accurately I used this computer software. All the dynamical models are simulated as per the description presented in section III.

7.1.2 Results

Results are obtained from the numerical simulations using MATLAB. We also matched our results with the iterative solution from the analysis of the dynamical models. From the results we can see that the nodes playing equivalent topological role also producing equivalent outcomes in the simulations of the dynamical scenarios. This is very significant because from the results we can see that the symmetry dominating over the other topological features like node degree. Based on these result we continued our study to the network quotients and we have seen a close matching between the quotient and full network simulation outcomes.

7.2 Future Research

My present study is limited to the undirected, unweighted networks but a number of real network is directed as well as weighted. So my present research can be extended for the directed and weighted networks. Besides, the future research scope from this study can be

- Perform physical experiments

- Study of approximate symmetry

- Finding appropriate scaling factor for quotient simulation

- Modification of the dynamic scenarios to incorporate the network quotients

7.3 Conclusion

In conclusion, my present research can introduce a new concept of analyzing the dynamical models in complex networks. This is very important because a good percentage of the real

networks have redundancy in terms of their topology. My current study emphasize on the reduction of these redundancy in complex networks in the study of the dynamical models.

References

[1] Cristopher Moore and Mark EJ Newman. Epidemics and percolation in small-world networks. *Physical Review E*, 61(5):5678, 2000.

[2] Juan G. Restrepo, Edward Ott, and Brian R. Hunt. Weighted percolation on directed networks. *Phys. Rev. Lett.*, 100:058701, Feb 2008.

[3] Ayalvadi Ganesh, Laurent Massoulié, and Don Towsley. The effect of network topology on the spread of epidemics. In *INFOCOM 2005. 24th Annual Joint Conference of the IEEE Computer and Communications Societies. Proceedings IEEE*, volume 2, pages 1455–1466. IEEE, 2005.

[4] David JD Earn, Pejman Rohani, Benjamin M Bolker, and Bryan T Grenfell. A simple model for complex dynamical transitions in epidemics. *Science*, 287(5453):667–670, 2000.

[5] Louis M Pecora, Francesco Sorrentino, Aaron M Hagerstrom, Thomas E Murphy, and Rajarshi Roy. Cluster synchronization and isolated desynchronization in complex networks with symmetries. *Nature communications*, 5:304–305, 2014.

[6] Louis M Pecora and Thomas L Carroll. Synchronization in chaotic systems. *Physical review letters*, 64(8):821, 1990.

[7] Hisashi Ohtsuki, Christoph Hauert, Erez Lieberman, and Martin A Nowak. A simple rule for the evolution of cooperation on graphs and social networks. *Nature*, 441(7092):502–505, 2006.

[8] Jörgen W Weibull. *Evolutionary game theory*. MIT press, 1997.

[9] David Arrowsmith, Mario di Bernardo, and Francesco Sorrentino. Communication models with distributed transmission rates and buffer sizes. In *Circuits and Systems, 2006. ISCAS 2006. Proceedings. 2006 IEEE International Symposium on*, pages 4–pp. IEEE, 2006.

References

[10] David Arrowsmith, Mario Di Bernardo, and Francesco Sorrentino. Effects of variations of load distribution on network performance. In *Circuits and Systems, 2005. ISCAS 2005. IEEE International Symposium on*, pages 3773–3776. IEEE, 2005.

[11] Mario di Bernardo and Francesco Sorrentino. Network structural properties, communication models and traffic dynamics. *Nolta*, 2006.

[12] Romualdo Pastor-Satorras and Alessandro Vespignani. Epidemic spreading in scale-free networks. *Physical review letters*, 86(14):3200, 2001.

[13] Albert-László Barabási and Réka Albert. Emergence of scaling in random networks. *science*, 286(5439):509–512, 1999.

[14] Mark EJ Newman. Mixing patterns in networks. *Physical Review E*, 67(2):026126, 2003.

[15] Mark EJ Newman. Assortative mixing in networks. *Physical review letters*, 89(20):208701, 2002.

[16] Michelle Girvan and Mark EJ Newman. Community structure in social and biological networks. *Proceedings of the national academy of sciences*, 99(12):7821–7826, 2002.

[17] Wayne W Zachary. An information flow model for conflict and fission in small groups. *Journal of anthropological research*, pages 452–473, 1977.

[18] The internet topology zoo.

[19] Osame Kinouchi and Mauro Copelli. Optimal dynamical range of excitable networks at criticality. *Nature physics*, 2(5):348–351, 2006.

[20] Ben D MacArthur, Rubén J Sánchez-García, and James W Anderson. Symmetry in complex networks. *Discrete Applied Mathematics*, 156(18):3525–3531, 2008.

[21] Ben D MacArthur and Rubén J Sánchez-García. Spectral characteristics of network redundancy. *Physical Review E*, 80(2):026117, 2009.

[22] Martin Golubitsky and Ian Stewart. *The symmetry perspective: from equilibrium to chaos in phase space and physical space*, volume 200. Springer Science & Business Media, 2003.

[23] Martin Golubitsky, Ian Stewart, et al. *Singularities and groups in bifurcation theory*, volume 2. Springer Science & Business Media, 2012.

[24] Francesco Sorrentino, Louis M Pecora, Aaron M Hagerstrom, Thomas E Murphy, and Rajarshi Roy. Complete characterization of stability of cluster synchronization in complex dynamical networks. *Science Advances 2*, 2015.

References

[25] SageMath - a free open-source mathematics software.

[26] Simon Knight, Huan X Nguyen, Nick Falkner, Richard Bowden, and Matthew Roughan. The internet topology zoo. *Selected Areas in Communications, IEEE Journal on*, 29(9):1765–1775, 2011.

[27] Zhi-Xi Wu and Ying-Hai Wang. Cooperation enhanced by the difference between interaction and learning neighborhoods for evolutionary spatial prisoner's dilemma games. *Physical Review E*, 75(4):041114, 2007.

[28] Jing Wang, Bin Wu, Xiaojie Chen, and Long Wang. Evolutionary dynamics of public goods games with diverse contributions in finite populations. *Physical Review E*, 81(5):056103, 2010.

[29] Shaolin Tan, Jinhu Lu, Guanrong Chen, and David J Hill. When structure meets function in evolutionary dynamics on complex networks. *Circuits and Systems Magazine, IEEE*, 14(4):36–50, 2014.

[30] Andrew Pomerance, Edward Ott, Michelle Girvan, and Wolfgang Losert. The effect of network topology on the stability of discrete state models of genetic control. *Proceedings of the National Academy of Sciences*, 106(20):8209–8214, 2009.

[31] K.-I. Goh, B. Kahng, and D. Kim. Universal behavior of load distribution in scale-free networks. *Phys. Rev. Lett.*, 87:278701, 2001.

[32] Y.Moreno, R.Pastor-Satorras, A.Vasquez, and A.Vespignani. Critical load and congestion instabilities in scale-free networks. *cond-mat*, 1(0209474), 2002.

[33] Mauro Copelli and Paulo RA Campos. Excitable scale free networks. *The European Physical Journal B*, 56(3):273–278, 2007.

[34] Daniel B Larremore, Woodrow L Shew, Edward Ott, and Juan G Restrepo. Effects of network topology, transmission delays, and refractoriness on the response of coupled excitable systems to a stochastic stimulus. *Chaos: An Interdisciplinary Journal of Nonlinear Science*, 21(2):025117, 2011.

[35] Lucas S Furtado and Mauro Copelli. Response of electrically coupled spiking neurons: a cellular automaton approach. *Physical Review E*, 73(1):011907, 2006.

[36] Daniel B Larremore, Woodrow L Shew, and Juan G Restrepo. Predicting criticality and dynamic range in complex networks: effects of topology. *Physical review letters*, 106(5):058101, 2011.

References

[37] Katia Basso, Adam A Margolin, Gustavo Stolovitzky, Ulf Klein, Riccardo Dalla-Favera, and Andrea Califano. Reverse engineering of regulatory networks in human b cells. *Nature genetics*, 37(4):382–390, 2005.

[38] The caida group, the caida as relationships dataset, 2006.

[39] Duncan J Watts and Steven H Strogatz. Collective dynamics of âĂŸsmall-worldâĂŹnetworks. *nature*, 393(6684):440–442, 1998.

[40] Bureau of transportation statistics, north american transportation atlas data., 1997.

[41] Sigact, the theoretical computer science genealogy.

[42] Marián Boguñá, Romualdo Pastor-Satorras, Albert Díaz-Guilera, and Alex Arenas. Models of social networks based on social distance attachment. *Physical review E*, 70(5):056122, 2004.